Device physics of single layer organic light-emitting diodes

B. K. Crone, I. H. Campbell, P. S. Davids, D. L. Smith, C. J. Neef, and J. P. Ferraris

Citation: Journal of Applied Physics **86**, 5767 (1999); doi: 10.1063/1.371591
View online: https://doi.org/10.1063/1.371591
View Table of Contents: http://aip.scitation.org/toc/jap/86/10
Published by the American Institute of Physics

Articles you may be interested in

Organic electroluminescent diodes
Applied Physics Letters **51**, 913 (1987); 10.1063/1.98799

Charge injection and transport in single-layer organic light-emitting diodes
Applied Physics Letters **73**, 3162 (1998); 10.1063/1.122706

Nearly 100% internal phosphorescence efficiency in an organic light-emitting device
Journal of Applied Physics **90**, 5048 (2001); 10.1063/1.1409582

Very high-efficiency green organic light-emitting devices based on electrophosphorescence
Applied Physics Letters **75**, 4 (1999); 10.1063/1.124258

Charge injection in organic light-emitting diodes: Tunneling into low mobility materials
Applied Physics Letters **69**, 2270 (1996); 10.1063/1.117530

Space-Charge-Limited Currents in Organic Crystals
Journal of Applied Physics **33**, 205 (1962); 10.1063/1.1728487

PHYSICS TODAY
WHITEPAPERS
MANAGER'S GUIDE
Accelerate R&D with Multiphysics Simulation
READ NOW
PRESENTED BY

Device physics of single layer organic light-emitting diodes

B. K. Crone, I. H. Campbell,[a] P. S. Davids,[b] and D. L. Smith
Los Alamos National Laboratory, Los Alamos, New Mexico 87545

C. J. Neef and J. P. Ferraris
The University of Texas at Dallas, Richardson, Texas 75080

(Received 14 July 1999; accepted for publication 13 August 1999)

We present experimental and device model results for electron only, hole only, and bipolar organic light-emitting diodes fabricated using a soluble poly (*p*-phenylene vinylene) based polymer. Current–voltage ($I-V$) characteristics were measured for a series of electron only devices in which the polymer thickness was varied. The $I-V$ curves were described using a device model from which the electron mobility parameters were extracted. Similarly, the hole mobility parameters were extracted using a device model description of $I-V$ characteristics for a series of hole only devices where the barrier to hole injection was varied by appropriate choices of hole injecting electrode. The electron and hole mobilities extracted from the single carrier devices are then used, without additional adjustable parameters, to describe the measured current–voltage characteristics of a series of bipolar devices where both the device thickness and contacts were varied. The model successfully describes the $I-V$ characteristics of single carrier and bipolar devices as a function of polymer thickness and for structures that are contact limited, space charge limited, and for cases in between. We find qualitative agreement between the device model and measured external luminance for a thickness series of devices. We investigate the sensitivity of the device model calculations to the magnitude of the bimolecular recombination rate prefactor. © *1999 American Institute of Physics.*
[S0021-8979(99)05922-8]

I. INTRODUCTION

Organic light-emitting diodes (LEDs) are of interest for displays because they show promise for low cost, large area devices, and they are compatible with low processing temperatures and flexible substrates.[1–4] The simplest organic LED consists of a thin layer of organic material sandwiched between two metal contacts. The organic layer is not doped and the asymmetry of the contacts determines the diode nature of the device.[5] By using appropriate contacts, electrons or holes or both are efficiently injected. For bipolar structures, in which both electrons and holes can be efficiently injected, radiative recombination in the organic layer results in the emission of light. There has been much work done recently to understand the basic principles of organic LED operation.[4–11]

Our approach to studying the device physics of organic LEDs is to begin with simple devices in which we can separate, to as large a degree as possible, the fundamental processes of charge injection, transport, and recombination. The understanding gained from the simple devices can then be applied to more complex structures. In this article we report experimental and model results for single layer devices with the structure metal_A/MEH-PPV/metal_B (denoted metal_A/metal_B), where MEH-PPV stands for poly [2-methoxy, 5-(2′-ethyl-hexyloxy)-1,4-phenylene vinylene]. The metal contacts determine the energy barrier to injection of electrons and holes. Thus, the choice of metal contacts determines whether the device is electron only, hole only, or bipolar. Previous work has shown that a variety of metals form contacts to MEH-PPV with energy barriers that follow the ideal Schottky picture.[9] Metals with small work functions such as Ca or Sm provide a small barrier to injection of electrons, and large work function metals such as Pt or Au provide a small barrier to injection of holes. Al and Cu provide a large barrier to injection for both holes and electrons into MEH-PPV.

We first consider single carrier electron only and hole only devices in order to determine independently the carrier injection from various contacts and the carrier transport properties of MEH-PPV. In these devices recombination does not play a significant role and current is limited either by injection at the contacts or by space charge in the organic film.[12] The transport parameters are obtained using a device model description of current–voltage ($I-V$) characteristics. The measured current–voltage characteristics of bipolar devices with a variety of thicknesses and Schottky energy barriers are then described using the carrier mobilities extracted from single carrier devices without additional fitting parameters. The device model provides insight into the carrier density and electric field profiles in the devices. These quantities are difficult to directly probe experimentally. In bipolar devices recombination can play an important role in determining the current–voltage characteristics.[12] However, for the devices investigated here, the current–voltage characteristics have a weak dependence on the recombination rate. Recombination does affect the carrier density profiles, recombination density profiles, and luminance efficiencies.

[a]Electronic mail: campbell@lanl.gov
[b]Present address: Intel Corporation, Hillsboro, OR 97124-6497.

 © 1999 American Institute of Physics

We describe the measured $I-V$ characteristics using a device model, described in detail elsewhere, that considers charge injection from the metal into the organic by thermionic emission and a backflowing interface recombination which is the time reversed process of thermionic emission.[10] We find that for most cases of interest for organic LEDs these two currents are separately much larger than the net device current and that they establish quasithermal equilibrium at the injecting contacts. Charge transport is described by continuity equations, with electric field dependent carrier mobilities and a drift-diffusion form for the current coupled to Poisson's equation. Carrier recombination is bimolecular with a Langevin form for the kinetic coefficient. Except for the carrier mobility all the parameters used in the device model are constrained to lie within the error of independently measured values. We take carrier mobilities to have an electric field dependence of the Poole–Frenkel form: $\mu = \mu_0 e^{\sqrt{(E/E_0)}}$ where E is the electric field and μ_0 and E_0 are parameters describing the mobility. This form for the mobility has been seen in time of flight measurements on conjugated organic materials, and has been derived theoretically.[13–19] It has been directly seen in time of flight measurements of MEH-PPV.[20]

The device fabrication has been described previously. Fabrication and measurement of devices was done either under vacuum or in an argon glove box atmosphere. Except for the results discussed in Appendix C, all devices were fabricated using MEH-PPV from the same synthetic run and using processing conditions that were as nearly identical as possible. The device thickness was determined from profilometer measurements. Capacitance–voltage measurements verify that the devices are fully depleted and also provide a check of device thickness. The Schottky energy barriers to charge injection for a variety of metals into MEH-PPV have been determined by combining electroabsorption and internal photoemission measurements.[9] The Schottky energy barriers to electrons and holes used in the model calculations are as follows: Pt (holes 0.1 eV), Au (holes 0.2 eV), Cu (holes 0.7 eV), Al (electrons 1.3 eV), and Ca (electrons 0.1 eV). The Schottky energy barrier to injection for the carrier not listed is given by subtracting the Schottky barrier shown from the energy gap of MEH-PPV (2.4 eV). There is a built-in potential in the device given by the difference between the Schottky energy barriers of the contacts.

The article is organized as follows: in Sec. II we describe the single carrier device results, in Sec. III we describe the bipolar device results, recombination is discussed in Sec. IV, and in Sec. V we summarize our conclusions. In Appendix A, we consider the effect of recombination on a device where both carriers have good injection and equal mobilities. In Appendix B, we show that essentially the same results are obtained if we consider injection into electronic states at one energy level or into states with a Gaussian distribution of energy levels. In Appendix C, we discuss variations in carrier mobility that arise when using MEH-PPV starting material from different synthetic runs and different processing conditions.

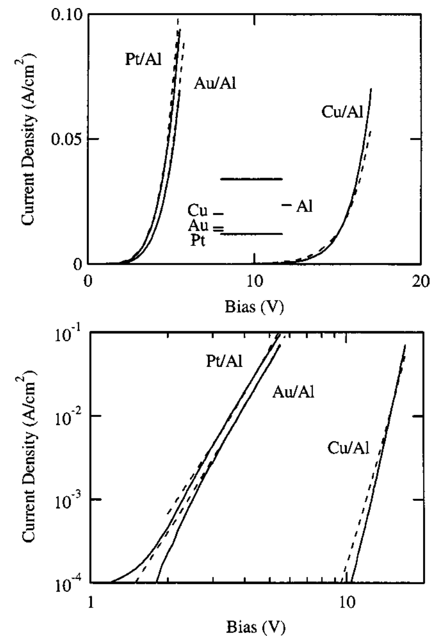

FIG. 1. Measured (solid line) and calculated (dashed line) current density vs bias voltage for Pt/Al, Au/Al, and Cu/Al hole only devices on linear (top panel) and log–log (bottom panel) scales. Holes are injected from the Pt, Au, and Cu electrodes. Devices are about 100 nm thick. The inset shows the relative energy levels.

II. SINGLE CARRIER DEVICES

In this section we present experimental and device model results for single carrier structures. A series of hole only devices is presented where the energy barrier for hole injection is varied by choosing different metal contacts. A thickness series of electron only devices were fabricated where Ca was always the electron injecting contact. The carrier density and electric field profiles calculated with the device model are presented for several of the devices.

Figure 1 shows current density versus bias voltage for Pt/Al, Au/Al, and Cu/Al hole only devices with about 100 nm thick MEH-PPV layers. The holes are injected from the Pt, Au, or Cu electrodes. The Al electrode provides a large barrier to electron injection. The experimental results are shown as solid lines and the model results as dashed lines. The hole mobility parameters $\mu_{0h} = 5\times10^{-8}\ \mathrm{cm^2 V\ s}$, and $E_{0h} = 1.3\times10^4$ V/cm were used for all the structures. Pt and Au provide space charge limited current because they have a small energy barrier for holes to MEH-PPV. Cu has a larger barrier and the current is limited by injection at the Cu/MEH-PPV contact. When the data and model results are plotted on a log–log scale, the data are approximately linear in all cases, although the current is not space charge limited for Cu/Al. The slope on the log–log plot is due to the field dependence of the mobility and the image force barrier lowering if the energy barrier to injection is large. The model describes the experimental data over several orders of magnitude in current density for a variety of Schottky energy barriers to injection.

Figure 2 shows current density versus bias voltage for a thickness series of Ca/Ca electron only devices. The experimental results are shown as solid lines and the model results

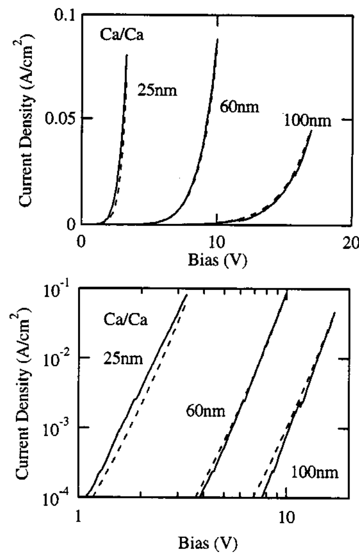

FIG. 2. Measured (solid line) and calculated (dashed line) current density vs bias voltage for 25-, 60-, and 100-nm thick Ca/Ca electron only devices on linear (top panel) and log–log (bottom panel) scales.

as dashed lines. The electron mobility parameters $\mu_{0e}=5\times10^{-12}\,\mathrm{cm^2/V\,s}$, and $E_{0e}=1.0\times10^4$ V/cm were used for all the structures. The current is space charge limited because the energy barrier to injection of electrons from Ca into MEH-PPV is small. The current is determined by bulk transport properties of the polymer. The model describes current–voltage characteristics for Ca/Ca devices over a range of thicknesses, and over several orders of magnitude of current density. The thickness scaling is not V^2/L^3 as predicted by the analytic calculation for space charge limited current that does not use field dependent mobilities.

Figure 3 shows the calculated carrier density and electric field profiles for contact limited (Cu/Al) and space charge limited (Pt/Al) hole only devices with 100- and 90-nm thick MEH-PPV layers, respectively. Profiles are shown for biases

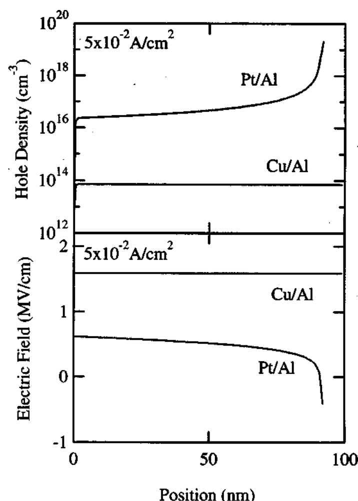

FIG. 3. Calculated hole density (top panel) and electric field (bottom panel) profiles for a 90 nm Pt/Al and a 100 nm Cu/Al device biased to provide 5×10^{-2} A/cm^2 device current density. The hole injecting contact is on the right.

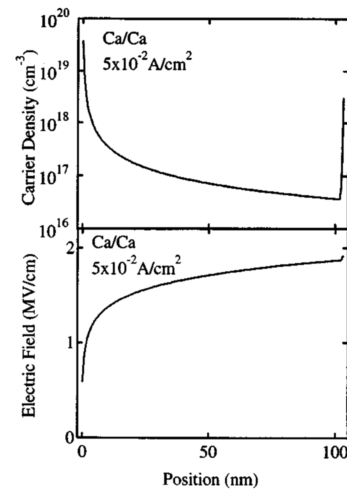

FIG. 4. Calculated electron density (top panel) and electric field (bottom panel) profiles for a 110 nm Ca/Ca device biased to provide 5×10^{-2} A/cm^2 device current density. The electron injecting contact is on the left.

that give a current density of 5×10^{-2} A/cm^2. In both cases the hole density at the injecting contact ($x=L$) is the quasithermal equilibrium value. For the Cu/Al device, there is a large barrier to injection for both holes and electrons so that the injected carrier densities are small and they do not significantly modify the electric field in the device. The carrier density and electric field are constant across the device. In the Pt/Al device the Pt contact has a small energy barrier to injection of holes so the hole density is high at this interface, causing a lowering of the electric field. The electric field and hole density vary across the device in such a way that the device current remains constant. The hole density in the Pt/Al device is over two orders of magnitude larger than the hole density in the Cu/Al device. The electric field is larger in the Cu/Al device and because of the strong field dependence of the carrier mobility, the μE product is over two orders of magnitude larger in the Cu/Al device and the device currents in the two structures are equal.

Figure 4 shows the calculated electron carrier density and electric field profile for the 100 nm Ca/Ca device at a bias such that the current density is 5×10^{-2} A/cm^2. The electron density at the injecting contact ($x=0$) is the quasithermal equilibrium value. The barrier to electron injection is small and sufficient space charge accumulates at the injecting contact to screen the electric field in this region. The Ca/Ca device is space charge limited for electrons.

III. BIPOLAR DEVICES

In this section we present experimental and device model results for bipolar single layer devices. Two device series are presented, a thickness series of Pt/Ca devices where both electron and holes are space charge limited, and a series where the electron injecting contact is always Ca, but the hole current is varied from contact limited to space charge limited. The current–voltage characteristics of these devices are measured and described with the device model using the carrier mobilities determined from the single carrier devices with no additional fitting parameters. The device

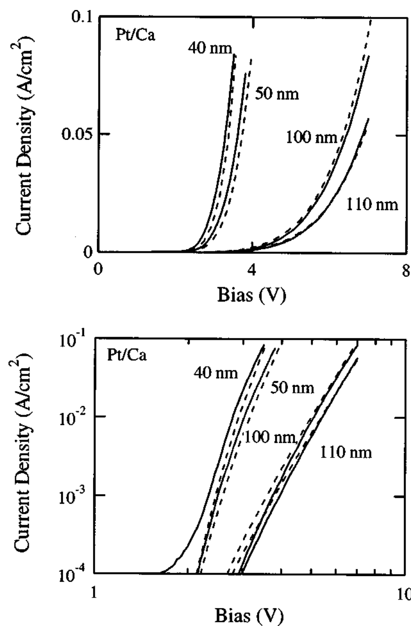

FIG. 5. Measured (solid line) and calculated (dashed line) current density vs bias voltage for 40-, 50-, 100- and 110-nm thick Pt/Ca bipolar devices on linear (top panel) and log–log (bottom panel) scales.

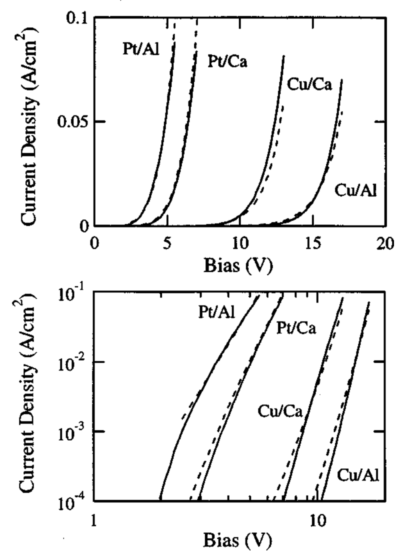

FIG. 6. Measured (solid line) and calculated (dashed line) current density vs bias voltage for Pt/Al and Cu/Al hole only devices and for Pt/Ca and Cu/Ca bipolar devices on linear (top panel) and log–log (bottom panel) scales. Holes are injected from the Pt, Au, and Cu electrodes. Electrons are injected from the Ca electrode. Devices are about 100 nm thick.

model assumes a bimolecular carrier recombination with a kinetic coefficient of the Langevin form, $R=\gamma np=e\mu_R np/\epsilon\epsilon_0$, where μ_R is the larger of the carrier mobilities, e is the electronic charge, $n(p)$ is the electron (hole) density, ϵ is the static dielectric constant, and ϵ_0 is the permittivity of free space.

Figure 5 shows current density versus bias voltage for a series of Pt/Ca bipolar devices with MEH-PPV layer thickness from 40 to 110 nm. The Pt and Ca contacts provide low energy barriers for hole and electron injection, respectively. The current is space charge limited and depends on bulk properties of the polymer. The data are described using the device model with carrier mobility parameters determined from the single carrier devices with no additional fitting parameters. The model describes the data over a range of device thickness and over several orders of magnitude of device current.

Figure 6 shows current density versus bias voltage for Pt/Ca and Cu/Ca bipolar devices, as well as Pt/Al and Cu/Al hole only devices. The Pt/Ca and Cu/Al devices are 100 nm thick, the Pt/Al is 90 nm thick, and the Cu/Ca is 80 nm thick. The Pt/Ca device has space charge limited current for electron and hole carriers, whereas the Cu/Ca device has space charge for electrons, but holes are contact limited due to the large energy barrier to injection of holes from Cu into MEH-PPV. The model describes the data well over several orders of current density using the mobility parameters determined from single carrier devices. The Pt/Ca and Pt/Al devices have similar currents, the Pt/Al current is somewhat higher because it is thinner and has a smaller built-in potential. The Cu/Ca device has a substantially larger current than the Cu/Al devices. This is due in part to the thickness difference, but primarily because the Cu/Ca device current has contributions from both electrons and holes, whereas the Cu/Al device current is hole only.

Figure 7 shows calculated carrier density and electric field profiles for Pt/Ca and Cu/Ca bipolar devices, for biases that give a current density of 6×10^{-2} A/cm^2. In both cases electrons are injected from the left at $x=0$ and holes from the right at $x=L$. The electron and hole densities are given by the quasithermal equilibrium values at the injecting contacts. For the Pt/Ca device the electrons and holes are space charge limited and have high carrier densities at the injecting contacts that suppress the electric field. The electron density drops rapidly across the device. The slope of this drop is determined by a combination of the electron mobility and carrier recombination. The holes dominate the current density across virtually the entire device. For the Cu/Ca device the electrons are space charge limited, but the holes are contact limited. The electric field and carrier densities near the

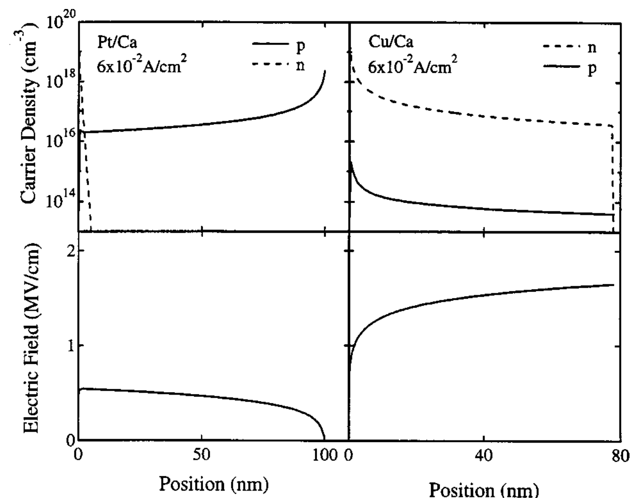

FIG. 7. Calculated hole (solid line) and electron (dashed line) carrier density and electric field profiles for Pt/Ca and Cu/Ca devices. The electron injecting contact is at the left and the hole injecting electrode is at the right.

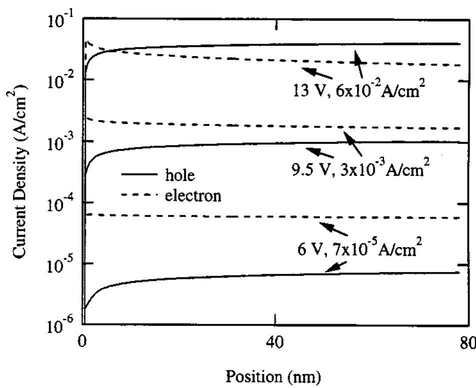

FIG. 8. Calculated electron (dashed line) and hole (solid line) current density profiles for a Cu/Ca device. The current density profiles are shown for bias voltages of 6, 9.5, and 13 V, corresponding to current densities of 0.07×10^{-5}, 3×10^{-3}, and 6×10^{-2}A/cm^2, respectively.

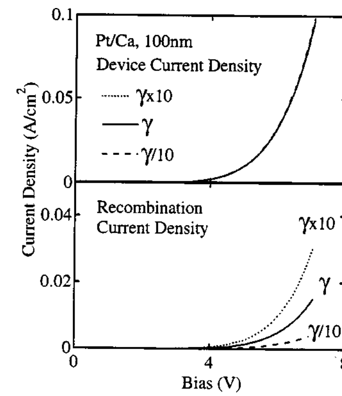

FIG. 9. Calculated device (top panel) and recombination (bottom panel) current density vs bias voltage for three values of γ, the kinetic coefficient of the recombination rate. Calculations are shown for the expected value of γ (solid line), and for the expected value of γ divided by (dashed line) and multiplied by (dotted line) a factor of 10.

hole injecting contact at $x=L$ are relatively constant. The electron density is high near the electron injecting contact at $x=0$, and screens the electric field. At this current density, the electron density is about three orders of magnitude larger than the hole density, however the electron mobility is about a factor of 300 lower than the hole mobility. The electrons and holes both contribute to the device current, as can be seen in Fig. 8 which shows calculated current density profiles for electrons and holes for the Cu/Ca device at applied biases of 6, 9.5, and 13 V, with current densities of 7×10^{-5}, 3×10^{-3}, and 6×10^{-2} A/cm^2, respectively.

IV. RECOMBINATION

In this section we address carrier recombination. Carrier recombination determines the light emission from a device, and also affects the current–voltage characteristics and carrier and field profiles. The model assumes a bimolecular Langevin recombination of the form $R=\gamma np$ with $\gamma=e\mu_R/\epsilon\epsilon_0$.[21] This is a total recombination rate, and includes both radiative and nonradiative processes. This recombination rate can be integrated across the device to give a net recombination current density J_r

$$J_r=\int_0^L eR\,dx=J_n(L)-J_n(0)=J_p(0)-J_p(L), \qquad (1)$$

where $J_n(x)[J_p(x)]$ is the electron [hole] current density as a function of position. This recombination current density can be used to calculate a device luminance by multiplying it by the optical energy gap, and by the fraction of recombination events that lead to external photon emission.

Figure 9 shows calculated current density (top) and recombination current density (bottom) versus applied bias for a 100 nm Pt/Ca device. Three values for the recombination rate kinetic coefficient are used; one tenth the Langevin value (dashed line), the Langevin value (solid line), and ten times the Langevin value (dotted line). The device current is essentially the same for all three cases. The recombination current increases (decreases) by a factor of 2 when the kinetic coefficient is increased (decreased) by a factor of 10. The recombination current is proportional to the light output.

Figure 10 shows calculated electron (upper panel) and hole (lower panel) density profiles for 100 nm Pt/Ca devices for the three values of the recombination rate kinetic coefficient: one tenth the Langevin value (dashed line), the Langevin value (solid line), and ten times the Langevin value. The carrier densities vary with γ predominantly near the Ca electron injecting contact at $x=0$. This region is shown in greater detail in the insets. When the kinetic coefficient is increased, both the electron and hole density decrease near the Ca contact. The hole density is relatively unaffected away from this contact. The device current in Pt/Ca devices is predominantly due to holes, so it is insensitive to the kinetic coefficient. The recombination is dominated by the region near the Ca contact, where the np product is appreciable.

The upper panel of Fig. 11 shows the measured and calculated external luminance versus device current for 40- and 110-nm thick Pt/Ca devices. The symbols are the measured device luminance using a silicon photodiode placed

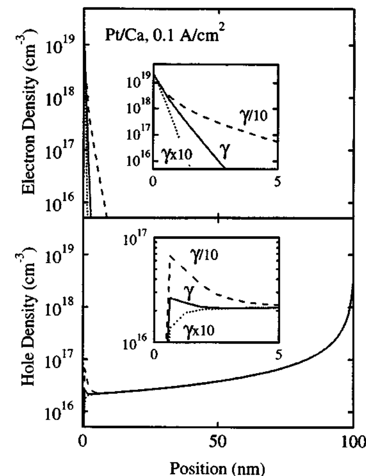

FIG. 10. Calculated electron (top panel) and hole (bottom panel) carrier density profiles for three values of γ, the kinetic coefficient of the recombination rate. Calculations are shown for the expected value γ (solid line), and for the expected value of γ divided by (dashed line) and multiplied by (dotted line) a factor of 10. The electron injecting contact is at the left and the hole injecting electrode is at the right.

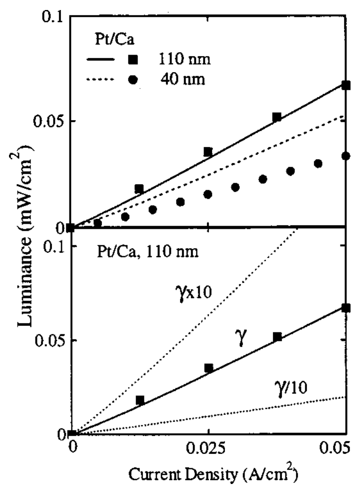

FIG. 11. Measured (symbols) and calculated (lines) external luminance vs device current density for 40- and 110-nm thick Pt/Ca devices (upper panel). Measured external luminance vs device current density for the 110 nm Pt/Ca device (symbol) and calculated external luminance for the same device for the expected value of γ (solid line), and for the expected value of γ divided by (dashed line) and multiplied by (dotted line) a factor of 10.

flush against the LED substrate. The lines are calculated external luminance obtained by multiplying J_r by the optical energy gap and by a factor ζ which is the fraction of recombination events leading to externally measurable light emission. The optical gap is 2.4 eV for MEH-PPV, and ζ was chosen as $\zeta=1/110$ so the measured and calculated luminance agreed for the 110 nm device. The model reproduces the linear behavior of luminance versus current density, and the decrease in luminance with decreasing device thickness. However, the model underestimates the magnitude of the luminescence drop with decreasing thickness. The lower panel shows the calculated external luminance versus device current for a 110-nm-thick Pt/Ca device using $\zeta=1/110$, and for recombination rate kinetic coefficient: of one-tenth the Langevin value (dashed line), the Langevin value (solid line), and ten times the Langevin value. A factor of 10 change in the recombination rate results in a factor of 2 change in the calculated luminance.

The factor ζ is determined by the photoluminescence yield, the fraction of excitons which are singlets, cavity effects, losses to the metal contact such as dipole quenching, reabsorption of the emitted light, and the fraction of generated photons which can escape the device.[22–25] A simple estimate of ζ can be obtained by neglecting cavity effects, reabsorption of the emitted light, and luminescence quenching by the metal contacts. The photoluminescence yield is about 15% for MEH-PPV. The fraction of excitons that are singlets is assumed to be 25%. The light emitted through the semitransparent metal, T, is the transmission coefficient of the contact. The light that escapes from the device is $(1-\cos\theta_c)$, where $\sin\theta_c=1/n$, and n is the refractive index of the material where the light is generated. For the devices considered here $T=0.25$ for the semitransparent Pt contacts, and $n=1.7$, so $\zeta\approx 1/600$. This value is about five times smaller than the value required to fit the data, so either the device model underestimates the amount of light emitted, or the simple model for ζ overestimates the losses.

V. CONCLUSION

The current–voltage characteristics of electron only and hole only single layer MEH-PPV devices were presented. The results were described by a device model in which the Poole–Frenkel form was used for the carrier mobilities. The mobility parameters extracted were $\mu_{0h}=5\times10^{-8}\,\mathrm{cm^2/V\,s}$ and $E_{0h}=1.3\times10^4\,\mathrm{V/cm}$ for holes, and $\mu_{0e}=5\times10^{-12}\,\mathrm{cm^2/V\,s}$ and $E_{0e}=1.0\times10^4\,\mathrm{V/cm}$ for electrons. As discussed in Appendix C, the carrier mobilities can change significantly for different synthetic runs of MEH-PPV. The model describes cases from contact limited to space charge limited over several orders of current density, and also describes the length scaling for space charge limited devices. Calculated carrier density and electric field profiles were shown for single carrier devices. The carrier densities at the injecting contacts were found to be the quasithermal equilibrium values. For the same current density, contact limited cases had carrier densities several orders of magnitude lower than those in space charge limited devices, however the electric field was only several times larger. This is the case because the field dependence of the carrier mobilities gives a very large increase in mobility for a severalfold increase in field.

Experimental and device model results were presented for bipolar single layer devices. Bipolar devices were measured and described with a device model using carrier mobilities determined from single carrier devices, and Schottky energy barriers and device thicknesses which were measured independently. The model accurately describes bipolar devices, both for a thickness series of Pt/Ca devices, and devices with Cu/Ca contacts, over several orders of magnitude in current density, without additional fitting parameters. In all cases the calculated carrier densities at the injecting contacts were found to be the quasithermal equilibrium values.

The calculated current–voltage characteristics of Pt/Ca LEDs are relatively insensitive to the magnitude of the prefactor chosen for recombination. Variations of recombination rate predominantly affect the carrier with a lower density. For Pt/Ca devices this is the low mobility electrons which do not contribute significantly to the device current over most of the device. The current–voltage characteristics for Cu/Ca devices are also relatively insensitive to changes in recombination rate. In this case it is because the low density holes are limited not by recombination, but rather by injection from the Cu electrode. For Pt/Ca devices the calculated recombination current is sensitive to the recombination rate, and is a measure of the light output by the device. Luminance was measured for a thickness series of Pt/Ca devices, and was described qualitatively with the device model. The model reproduces the linear dependence of luminance on current density, and showed a decrease in the magnitude and slope of the luminance versus current density as the device thickness decreases.

ACKNOWLEDGMENTS

The authors thank D. R. Brown for technical assistance. This work was partially funded by the Los Alamos National Laboratory LDRD program.

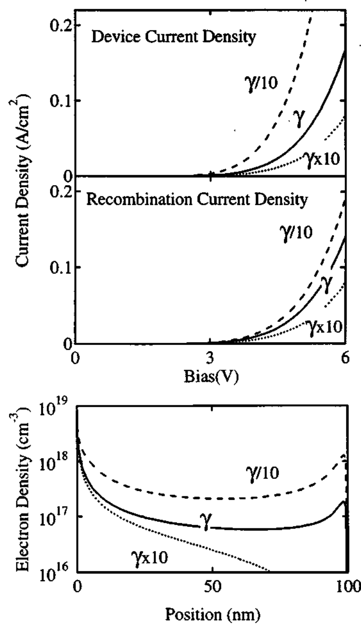

FIG. 12. Calculated device (top panel) and recombination (middle panel) current density vs bias voltage, and electron density profile (bottom panel) for three values of γ, the kinetic coefficient of the recombination rate. Calculations are shown for the expected value of γ (solid line), and for the expected value of γ divided by (dashed line) and multiplied by (dotted line) a factor of 10.

APPENDIX A: EFFECT OF RECOMBINATION ON MATERIALS WITH EQUAL CARRIER MOBILITIES

The MEH-PPV used in this work has a much larger hole than electron mobility. The calculated current density was found to be insensitive to the magnitude of the prefactor γ of the recombination rate. For cases with good injection of both carriers such as Pt/Ca, the current is dominated by the high mobility holes, whereas changes in γ predominantly affect the low mobility electrons near the electron injecting contact where the np product is appreciable. For cases where both carriers contribute to the current density such as Cu/Ca devices, the hole density is low across the entire device, so the recombination rate is low. However, for materials in which the two carriers have nearly the same mobility, recombination can have a significant influence on the current–voltage relations. To illustrate this point we consider 100-nm thick devices with an organic material in which the carrier mobilities are equal with $\mu_0 = 5\times10^{-8}\,\mathrm{cm^2/V\,s}$, and $E_0 = 1.3\times10^4$ V/cm, and both carriers are space charge limited with a 0.2 eV energy barrier to injection. Figure 12 shows current density versus applied voltage (upper panel), recombination current versus applied voltage (middle panel), and electron density profile (lower panel) for recombination rate kinetic coefficients of: one tenth the Langevin value (dashed line), the Langevin value (solid line), and ten times the Langevin value (dotted line). The hole density is the mirror image of the electron density. The calculated device and recombination current density, and the carrier densities all increase as the recombination rate decreases. The electron and hole densities increase as recombination is reduced, however the total charge and electric field remain unchanged. The higher carrier densities balance each other to satisfy Poisson's equation, and lead to higher device current densities. The recombination current density also increases with decreasing recombination prefactor, however the ratio of recombination current to device current decreases with decreasing recombination as expected. The results presented for MEH-PPV showed that the device current for Pt/Ca and Cu/Ca devices was relatively independent of the magnitude of γ. Here we have shown that the calculated current densities are more sensitive to γ for materials with equal carrier mobilities.

APPENDIX B: INJECTION INTO A GAUSSIAN DENSITY OF STATES

The results presented above assume carrier injection into a single electronic energy level in the organic material at room temperature. In this section we will show that these results do not change significantly when a Gaussian distribution of energy levels in the organic material is considered. For essentially all cases of interest the carrier density at the injecting contacts is given by quasithermal equilibrium values, thus we need to consider how broadening the energy levels into a Gaussian changes the quasithermal equilibrium carrier density at the interface. For a single energy level, the quasithermal equilibrium carrier density at the interface in the nondegenerate case is

$$n(0) = N_0 e^{-(\epsilon_0-\epsilon_f)/kT}, \tag{B1}$$

where N_0 is the density of states of the organic material, ϵ_0 is the energy of the states, ϵ_f is the quasi-Fermi level at the interface, k is Boltzmann's constant, and T is the temperature. If we consider a Gaussian density of states centered at ϵ_0 with variance σ,

$$D(\epsilon) = N_0 \frac{1}{\sqrt{2\pi\sigma^2}} e^{-(\epsilon-\epsilon_0)^2/\sigma^2}, \tag{B2}$$

the quasithermal equilibrium carrier density at the interface in the nondegenerate case is

$$n(0) = N_0 e^{-(\epsilon_0-\epsilon_f)/kT} e^{\sigma^2/2kT}. \tag{B3}$$

Equation (B3) can be written as

$$n(0) = N_0 e^{-(\epsilon_0^{\mathrm{eff}}-\epsilon_f)/kT}, \tag{B4}$$

where

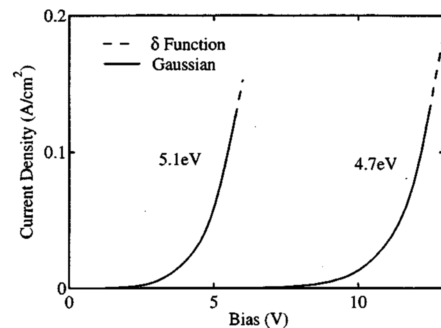

FIG. 13. Calculated current density vs bias voltage for injection into a single δ-function level (solid line) and a Gaussian distribution of states (dashed line). Calculations are shown for a hole injecting electrode work function of 4.7 eV (contact limited) and 5.1 eV (space charge limited).

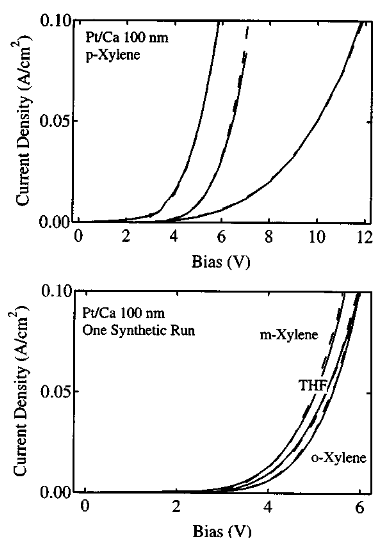

FIG. 14. Measured (solid line) and calculated (dashed line) current density vs bias voltage for 100-nm thick Pt/Ca devices made using MEH-PPV from three different synthetic runs spin cast from *p*-xylene solutions (top panel) and from one synthetic run spin cast using different solvents (bottom panel). The variation from synthetic run to synthetic run is much greater than that due to different solvents.

$$\epsilon_0^{\text{eff}} = \epsilon_0 - \sigma^2/2kT. \tag{B5}$$

For a given temperature the solution for a Gaussian density of states is equivalent to the result for a single level at an effective energy given by Eq. (B5). For typical values of the variance the shift at room temperature is smaller than the uncertainty in the determination of the energy levels.

Figure 13 shows the calculated current density versus applied voltage for a hole only 100 nm device for injection into a single electronic layer (solid line) and into a Gaussian density of states (dashed line). Two values of the Fermi energy for the hole injecting contact are considered, 5.1 eV for a space charge limited contact, and 4.7 eV for a contact limited contact. The discrete energy level of the organic electronic state in the single level case is 5.3 eV. The variance of the Gaussian is 70 meV. The center of the Gaussian is shifted compared to the discrete level by 94 meV. The current densities calculated from either single energy levels or Gaussian densities of states are essentially the same for both contact limited and space charge limited cases.

APPENDIX C: STARTING MATERIAL AND PROCESSING EFFECTS ON MOBILITY PARAMETERS

All of the devices discussed above were fabricated using MEH-PPV from a single synthetic run and using processing conditions that were as nearly identical as possible. The electrical properties of the MEH-PPV films can vary significantly when using MEH-PPV from different synthetic runs or using different processing conditions. Figure 14 (top panel) shows measured and calculated current–voltage characteristics of 100-nm thick Pt/Ca devices made using MEH-PPV from three different synthetic runs all spun from *p*-xylene solutions. For the three runs shown the μ_{0h} values range from 5×10^{-8} cm^2/V s to 1.4×10^{-6} cm^2/V s and the E_{0h} values range from 1.3×10^4 V/cm to 1×10^5 V/cm. Figure 14 (bottom panel) shows the measured and calculated current–voltage characteristics of 100-nm thick Pt/Ca devices when using a single synthetic run and different solvents. The μ_{0h} values range from 1.65×10^{-7} cm^2/V s to 6.25×10^{-7} cm^2/V s and the E_{0h} values range from 1.1×10^4 V/cm to 2×10^4 V/cm. The observed variation from synthetic run to synthetic run is much greater than that due to different solvents. The origin of the significant run to run variation is not clear but may be related to the solubility of the polymer that is sensitive to its molecular weight distribution.

[1] C. W. Tang and S. A. VanSlyke, Appl. Phys. Lett. **51**, 913 (1987).
[2] J. H. Burroughes, D. D. C. Bradley, A. R. Brown, R. N. Marks, K. Mackay, R. H. Friend, P. L. Burns, and A. B. Holmes, Nature (London) **347**, 539 (1990).
[3] D. Braun and A. J. Heeger, Appl. Phys. Lett. **58**, 1982 (1991).
[4] N. C. Greenham and R. H. Friend, Solid State Phys. **49**, 1 (1995).
[5] D. Braun, A. J. Heeger, and H. Kroemer, J. Electron. Mater. **20**, 945 (1991).
[6] E. M. Conwell and M. W. Wu, Appl. Phys. Lett. **70**, 1867 (1997).
[7] P. W. M. Blom, M. J. M. deJong, and S. Breedijk, Appl. Phys. Lett. **71**, 930 (1997).
[8] I. D. Parker, J. Appl. Phys. **75**, 1656 (1994).
[9] I. H. Campbell, T. W. Hagler, and D. L. Smith, Phys. Rev. Lett. **76**, 1900 (1996).
[10] P. S. Davids, I. H. Campbell, and D. L. Smith, J. Appl. Phys. **82**, 6319 (1997).
[11] P. W. M. Blom and M. J. M. deJong, IEEE J. Sel. Top. Quantum Electron. **4**, 105 (1998).
[12] M. A. Lampert and P. Mark, *Current Injection in Solids* (Academic, New York, 1970).
[13] D. M. Pai, J. Chem. Phys. **52**, 2285 (1970).
[14] H. Bässler, Phys. Status Solidi B **175**, 15 (1993).
[15] Yu. N. Garstein and E. M. Conwell, Chem. Phys. Lett. **245**, 351 (1996).
[16] D. H. Dunlap, P. E. Parris, and V. M. Kenkre, Phys. Rev. Lett. **77**, 542 (1996).
[17] H. Meyer, D. Haarrer, H. Naarmann, and H. H. Horhold, Phys. Rev. B **52**, 2587 (1995).
[18] R. G. Kepler, P. M. Beeson, S. J. Jacobs, R. A. Anderson, M. B. Sinclair, V. S. Valencia, and P. A. Cahill, Appl. Phys. Lett. **66**, 3618 (1995).
[19] M. Abkowitz, J. S. Facci, and M. Stolka, Chem. Phys. **177**, 783 (1996).
[20] I. H. Campbell, D. L. Smith, C. J. Neef, and J. P. Ferraris, Appl. Phys. Lett. **74**, 2809 (1999).
[21] V. N. Abakumov, V. I. Perel, and I. N. Yassievich, *Nonradiative Recombination in Semiconductors* (North-Holland, Amsterdam, 1991), p. 108.
[22] N. C. Greenham, I. D. W. Samuel, G. R. Hayes, R. T. Phillips, Y. A. R. R. Kessener, S. C. Morati, A. B. Holmes, and R. H. Friend, Chem. Phys. Lett. **241**, 89 (1995).
[23] R. R. Chance, A. Prock, and R. Silbey, Adv. Chem. Phys. **37**, 1 (1979).
[24] H. Becker, A. Lux, A. B. Holmes, and R. H. Friend, Synth. Met. **85**, 1289 (1997).
[25] S. E. Burns, N. C. Greenham, and R. H. Friend, Synth. Met. **76**, 205 (1996).